# How many bits in a single magnetic dot?

Fabien Cheynis, Olivier Fruchart, Jean-Christophe Toussaint, Nicolas Rougemaille, Rachid Belkhou

# How many bits in a single magnetic dot?

F. Cheynis,[1,2] O. Fruchart,[1,*] J. C. Toussaint,[1,2] N. Rougemaille,[1] and R. Belkhou[3,4]

[1] *Institut NÉEL, CNRS & Université Joseph Fourier – BP166 – F-38042 Grenoble Cedex 9 – France*
[2] *Institut National Polytechnique de Grenoble – France*
[3] *Synchrotron SOLEIL, L'Orme des Merisiers Saint-Aubin - BP 48, F-91192 Gif-sur-Yvette Cedex, France*
[4] *ELETTRA, Sincrotrone Trieste, I-34012 Basovizza, Trieste, Italy*

(Dated: December 22, 2007)

Digital information processing relies on the handling of two states, called bits or '0' and '1'. In magnetoelectronic devices bits are stored using the two possible directions of magnetization in nanoscale bistable domains. In hard-disk drives these are written in continuous thin films, while in Magnetic Random Access Memories (MRAMs) or for other concepts of magneto-logic devices[1] bits rely on single-domain flat elements patterned with lithography. While miniaturisation is the conventional way to fuel the continuous increase of device density, disruptive solution are also sought. For patterned elements, *e.g.* disk-shaped, it has been proposed that bits could be stored in dots displaying a flux-closure magnetic state, coded in the chirality of the structure[2] or in the up-or-down magnetic vortex at the center of the dot[3]. In this Letter we go one step further, and show numerically and experimentally that a third bit, *i.e.* implying in principle eight independent micromagnetic states, could be stored in a simple magnetic dot. This is achieved by considering an elongated dot, in which case the vortex is replaced by a more complex domain wall displaying two internal degrees of freedom.



To illustrate how two distinct magnetic degrees of freedom can be addressed in a single magnetic dot, let us consider a square and flat element (the same qualitative discussion also applies to the more common disk-shaped element). In such an element the magnetization lies in-the-plane and spontaneously curls to follow the edges and close the magnetic flux lines, as this allows to reduce the magnetostatic, *i.e.* dipole-dipole, energy (FIG. 1a-b). The chirality can be clockwise or anticlockwise. In the very center of the dot the magnetization must point out-of-the-plane, in order to lift the singularity of exchange energy that would otherwise occur owing to the in-plane curling. This central region is called a magnetic vortex. A vortex has a diameter roughly equal to 10 nm[4] and can equally point upwards or downwards. This flux-closure state is named after it a *vortex state*. Thus a square or disk-shaped magnetic element in a vortex state contains two micromagnetic degrees of freedom: its chirality and the polarity of the vortex core. The chirality can be controlled introducing some asymmetry in the dot[5], or alternatively by applying a locally non-uniform magnetic field to a symmetric dot[2]. The core polarity can be reversed using a high, out-of-plane magnetic field ($\approx 0.4$ T), without affecting the vorticity[6,7]. Very recently the reversal of the vortex core could be achieved, still without affecting the chirality, applying an in-plane magnetic field of much smaller magnitude, typically 1 mT. This value becomes perfectly relevant for devices. This small magnitude was made possible by the use a field pulsed at the nanosecond time scale[8,9,10]. Thus the two degrees of freedom in a micromagnetic vortex state could be used as two independent bits for fast, low consumption and high density solid-state magnetic devices in the future.

What becomes of the magnetic vortex if we now consider a dot with an elongated shape is illustrated by numerical simulation (see *Methods* section) in FIG. 1c-d. The vortex is replaced with a domain wall aligned in the direction of the long axis of the dot. For a dot thickness larger than a few tens of nanometers the magnetization in the core of the wall remains in the plane of the wall, *i.e.* perpendicular to the surface of the element. This arrangement is called a Bloch wall. However contrary to the text-book case where a translational symmetry is assumed in the wall plane, at both dot interfaces (dot/substrate and cover-layer/dot) the Bloch wall is terminated by an area with in-plane magnetization (FIG. 1e)[11,12]. Such areas are now often called Néel caps[13] because the domain wall profile at each surface mimics the profile of a conventional Néel wall, a type of domain wall with solely in-plane magnetization and usually found in magnetic ultrathin films[14]. The reason for the occurrence of Néel caps is again the minimization of the dipolar energy, achieved by closing as much as possible the lines of magnetic flux. This overall arrangement is called an asymmetric Bloch wall. Its has been described in details first in thin films[12] and more recently in nanostructures[15,16,17,18,19]. Notice that conceptually the asymmetric Bloch wall can be derived from a vortex without topological modifications, by pulling in opposite directions its top and bottom extremities (FIG. 1b,d). For convenience, in the following we will name these extremities *surface vorticies*. This conceptual way of building a Bloch wall implies a breaking of symmetry[15], *i.e.* the top vortex may be pulled towards $+x$ or $-x$. As shown below, this breaking of symmetry gives rise to two possible orientations of the top Néel cap, while the bottom cap remains antiparallel to the top one. These bistable states for the set of the two antiparallel Néel caps is thus

*Olivier.Fruchart@grenoble.cnrs.fr

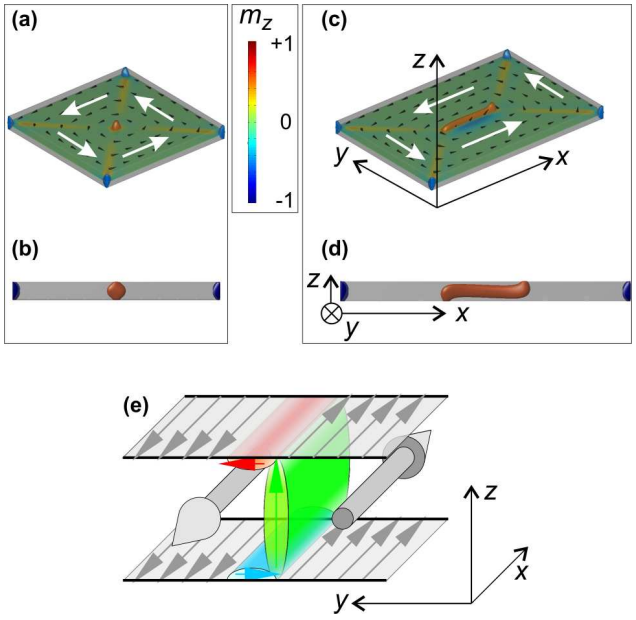


FIG. 1: **General features of domain walls in square and rectangular magnetic elements.** (a) top view and (b) cross section of a so-called *vortex* state in a square magnetic element ($500\times500\times50$ nm). (c) top view and (d) cross section of a so-called *Landau* state in a rectangular magnetic element ($700\times500\times50$ nm). Only areas with normalized perpendicular magnetization $m_z$ higher than 0.5 are displayed, with a view to highlighting the vortex and the domain wall. In (a-b) the map of $m_z$ at mid-height is also shown, where the in-plane direction of magnetization is indicated by white arrows. The bar indicates the color code for $m_z$. (e) Schematic view of a Bloch domain wall terminated by a *Néel cap* at each surface. The in-plane domains are oriented along the $+x$ and$-x$ axes on either side of the wall (grey arrows). The magnetization in the core of the Bloch wall lies along the $z$ axis, *i.e.* within the plane of the wall and perpendicular to the nanostructure. The magnetization is opposite in the top and bottom Néel caps, and points along the $\pm y$ axes, *i.e.* across the plane of the wall.

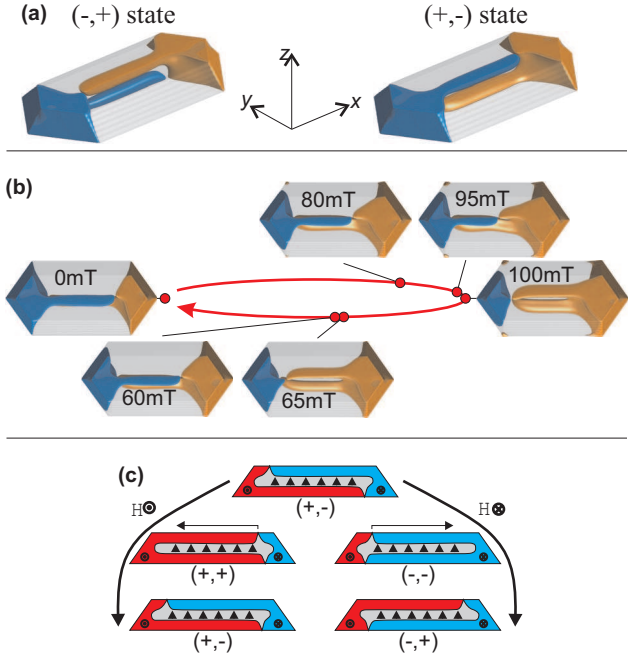


FIG. 2: **Micromagnetic simulations in a** 100 nm**-thick, elongated magnetic dot.** (a) $(-,+)$ and $(+,-)$ states, as defined with respect to the orientation of the bottom and top Néel cap along the $y$ axis. In this open view, we display as volumes only the areas with normalized transverse magnetization larger than 0.5 in absolute value. Positive and negative values appear red and blue, respectively. (b) Hysteresis of Néel caps during a magnetization process in positive field starting from a $(+,-)$ state (c) Cross section view of magnetization processes starting from a $(+,-)$ initial state: when the magnetic field is removed , only the top Néel cap reverses, stabilizing a $(-,+)$ or '$(+,-)$ final state depending on the direction of the applied field.

an extra degree of freedom that does not exist in the case of a vortex state. Notice that in such elongated dots the chirality can still be defined as the sense of rotation of the in-plane magnetization around the domain wall (*e.g.* anticlockwise in FIG. 1d). The orientation of magnetization in the core of the Bloch wall may also point either 'up' or 'down'. Altogether such an elongated dot is described by three micromagnetic degrees of freedom instead of two in the standard vortex state. In the following, we show numerically and experimentally that this third degree of freedom can be switched using a magnetic field, without affecting the two other degrees of freedom.

Using micromagnetic simulations we now investigate the magnetic behavior of a 100 nm-thick magnetic Fe dot (FIG. 2). The geometrical features of the dot have been set similar to those of the microstructures used experimentally (see below and Methods section). For a given in-plane chirality and a given polarity of the core of the Bloch wall, two degenerate magnetic ground states are found at zero external field, depending on the set of antiparallel Néel caps. We name these states after the $y$-orientation of the bottom and top Néel caps respectively, *i.e.* $(-,+)$ and $(+,-)$ (FIG. 2a). Starting from an initial $(+,-)$ state at remanence, we now apply a magnetic field $H_t$ along its short axis $y$. Upon applying a positive $H_t$ no change occurs up to 95 mT, except for a small and reversible shift of the Bloch wall along the length of the dot (FIG. 2b). When $H_t$ reaches 100 mT the top surface vortex runs through the entire Néel cap to finally settle essentially atop the bottom vortex. The two Néel caps are then parallel and aligned along the field [$(+,+)$ state]. This arrangement is sometimes named an *asymmetric Néel wall*. This is consistent with the findings in thin films that the asymmetric Néel wall is favored against the asymmetric Bloch wall when a transverse field is applied[4,20]. When decreasing $H_t$ back to zero, no significant change occurs down to 60 mT, where the surface vortex runs back to its initial position [$(+,-)$ state]. The

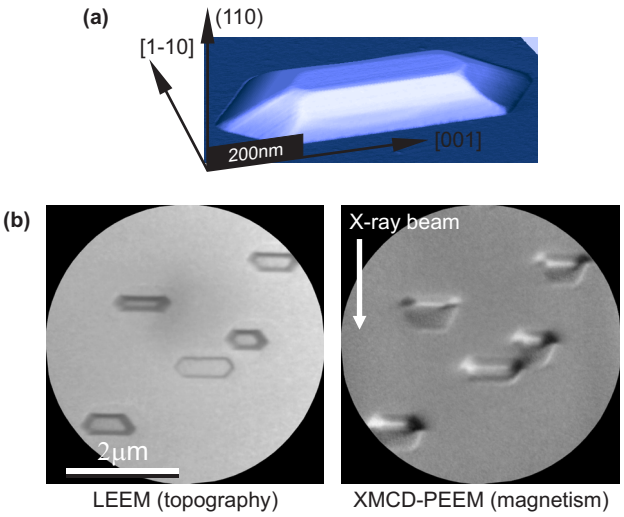


FIG. 3: **Experimental results.** (a) 3D view of a typical self-assembled epitaxial Fe(110) dot (Atomic force microscopy, true aspect ratios) . (b) A typical view of an assembly of dots imaged by the LEEM/PEEM microscope. After magnetization to −130 mT the dots are in the $(-,+)$ state at remanence whatever their size, height or asymmetry (see the white contrast for the Néel caps).

fact that the propagation field differs upon increasing or decreasing $H_t$ shows that the process is irreversible, as usually observed in conventional magnetization switching processes. Starting from the same initial $(+,-)$ state we now decrease the field to negative values. In this case the top Néel cap is unaffected, while it is the bottom surface vortex that runs through the dot at $H_t = 100$ mT (not shown here). Again, the system reaches a magnetic state with two parallel Néel caps aligned along the applied field [$(-,-)$ state]. Interestingly, when $H_t$ is reduced back to zero it is still the top Néel cap that switches back, leaving a $(-,+)$ state at remanence, *i.e.* opposite to the initial state. The fact that it is always the top Néel cap that switches back when the field is reduced towards zero remains an open question. The tilted facets, which break the symmetry between the top and bottom surfaces, may be involved. To summarize the results of numerical simulations, it is predicted that the top Néel cap at remanence is antiparallel to the applied transverse field: a positive (resp. negative) field selects the $(+,-)$ state [resp.$(-,+)$] (FIG. 2c). Notice that the states with parallel Néel caps, $(+,+)$ and $(-/-)$, are not stable under zero field, so that the Néel caps can be used to store one bit of information only, not two.

The micromagnetic predictions are confirmed experimentally. Single-crystalline micron-sized elongated Fe dots with a three-dimensional facetted shape and atomically-flat facets, have been prepared by self-assembly using a well-established procedure[21](FIG. 3a, and Methods). High resolution magnetic imaging of the in-plane component of the Néel cap surface magnetization was performed using X-PEEM (see FIG. 3b, and Methods section). Since no magnetic field can be applied while imaging, measurements were performed at remanence after *ex situ* application of a transverse magnetic field with a given magnitude. Imaging several tens of dots at each stage reveals that starting from equiprobable $(-,+)$ and $(+,-)$ configurations in the as-grown state, the occurrence of the $(+,-)$ state at remanence progressively increases as we increase the amplitude of the applied transverse magnetic field. The mean switching field derived from this series is $H_{sw} = 120$ mT with a $\pm 10$ mT distribution. The occurrence of the $(+,-)$ state reaches 95 % for $H_t = +150$ mT. Similarly, 95 % of $(-,+,)$ states are found after application of $H_t = -150$ mT. The value of the switching field ($H_{sw} = 120$ mT) determined experimentally is in good agreement with the numerical simulations presented above (100 mT).

In a quantitatively-similar picture, we have thus demonstrated numerically and experimentally that the direction of magnetization in Néel caps in elongated ferromagnetic dots can be switched reversibly using a transverse magnetic field. We stress that the switching mechanism does affect neither the chirality of the in-plane magnetic domains nor the polarity of the core of the domain wall. Whereas this conclusion comes straightforwardly in simulations, it requires some statistical analysis in the experiments as we do not image the same dots at different stages of the magnetization process (see Methods). This analysis reveals that, within the error bar related to the finite number of dots imaged at each magnetization stage, typically a few tens, the occurrence of clockwise and anticlockwise chiralities remains similar for all applied magnetic fields. No cross-correlation between the chirality and the state of the Néel caps could be evidenced either, still within the experimental error bars. In principle the polarity of the wall core may be determined examining the details of the surface magnetization pattern[22], however this could not be done reliably here because nearly half of the dot is invisible in XMCD-PEEM due to shadowing effects. Therefore we known from simulations only that the core of the wall remains unaffected. All these results unambiguously demonstrate that there are three truly independent degrees of freedom in a single magnetic element, or bits in terms of storage, whereas two only exist in the more common vortex state found in circular dots. Whether this third degree of freedom could be exploited in multi-level logic or solid-state storage devices remains an open question. A prerequisite is to demonstrate that the Néel caps can be manipulated at high frequency and with much smaller field magnitude than the 100 mT demonstrated here. This aim may not be non-realistic recalling that the field required to switch a vortex core could be reduced in a few years time from 0.4 T in the first demonstration[6] to about 1 mT nowadays[8,9,10]. The reversal could also be achieved using a radiofrequency spin-polarized current using the spin-transfer torque, a physical effect[23,24] promising an increased entanglement of magnetism and nanoelectron-

ics in the future[25]. Pathways to ease the switching of Néel caps include tailoring the field geometry and duration as for the vortex state, and also the dot's geometry or thickness. For practical purposes the dots may be fabricated with standard lithography techniques, as the use of self-assembled dots is not expected to play a role in the switching of the Néel caps. Finally notice that the working principle of our scheme is similar to that of the hysteron, where a patterned convex-concave elongated peanut shape was intended to induce two stable positions for a vortex. However this design was proven to potentially give rise to several metastable positions of the vortex for each state of the bit, which would result in practice in systematic signal noise[26]. This multiplicity of sub-states for the vortex location seems to be a general feature of geometrical constrictions and sharp turns in stripes[27]. Thus , from both the point of view of easiness of patterning and that of reliability, the scheme of a domain wall in an elongated dot with a fully convex shape is more promising.

## Methods

### A. Sample fabrication

The samples were fabricated at Institut Néel (Grenoble) using UHV pulsed-laser deposition, also called laser-MBE[28]. Details can be found in Ref.[21]. Atomic force microscopy was performed *ex situ* with a Park Autoprobe CP and a 100 $\mu$m lateral scanner. The samples consist of epitaxial self-assembled Fe dots. By self-assembly we refer to the bottom-up fabrication approach where the deposited atoms assemble spontaneously into dots during growth, with however no positional order arising between the dots. As a supporting surface we use $Al_20_3(11\bar{2}0)$ wafers provided by the Bicron company, buffered with a layer of W of crystallographic (110) orientation with high single-crystalline surface quality[21,29]. The dots display atomically-smooth top and various types of facets tilted with respect to the wafer plane. The anisotropy of these facets results in the dot elongation parallel to the in-plane crystallographic direction [001]. The dots' size can be adjusted varying deposition temperature and amount of material deposited[21]. Here the conditions were chosen so that the average length, width and height of the dots equals 1 $\mu$m, 0.5 $\mu$m and 0.1 $\mu$m, respectively. The dots are capped *in situ* with 0.7 nm-thick Mo followed by a 2.5 nm-thick Au layer as protective layer to prevent oxidation during the air sample transfer between the MBE chamber and the microscope.

### B. Micromagnetic simulations

The micromagnetic simulations were performed using GL_FFT, a custom-developed code based on a finite-differences scheme, *i.e.* the sample is discretized with a regular array of prisms. The magnetization vector at each node is estimated as a second-order interpolation of the vector field between the cell and its nearest neighbors, thus allowing the volume charges to vary linearly. The dipolar energy is calculated in the Fourier space. For this purpose we used the fast Fourier transform procedure developed by M. Frigs and S. G. Johnson, which is able to handle meshes with a number of cells equaling an arbitrary product of prime integers, not powers of two only[30]. The accuracy of our approach reaches the precision of the model B proposed by Ramstöck *et al.*[31]. In practice the dots were divided into cells with uniform lateral and vertical size $\Delta_x = \Delta_y = 3.9$ nm and $\Delta_z = 3.1$ nm, respectively. We set the magnetic properties equal to those of bulk Fe at 300 K, which from continuous films are known[32] to be free from finite-size effects for the large thicknesses considered here: magneto-cristalline fourth-order anisotropy constant $K_1 = 4.8\times10^4$ J/m$^3$, exchange energy $A = 2\times10^{-11}$ J/m and spontaneous magnetization $M_s = 1.73\times10^6$ A/m.

### C. XMCD-PEEM magnetic imaging

The high-resolution magnetic imaging experiments were performed on the Nanospectroscopy beamline (Elettra, Italy), using an Elmitec Gmbh commercial LEEM/PEEM microscope (LEEM V). In the Low Energy Electron Microscopy (LEEM) mode[33] electrons are balistically backscattered from the surface upon illumination by a low-energy electron beam, which are collected, magnified and projected onto a channelplate that is read by a CCD camera. The lateral resolution of the LEEM is better than 10 nm, and reveals the geometrical features of the studied objects. In the Photo-Emission Electron Microscope (PEEM) mode the microscope collected the secondary electrons emitted from the surface sample upon illumination by X-rays, in our case that are incident on the sample at an angle of 16° from the surface and form a 10 $\mu$m spot. The spatial resolution of the microscope in this photoemission mode (PEEM) is limited by the chromatic and spherical aberration to 25 nm, with a probing depth around 10 nm. The surface spin structure of the Neel cap has been determined taking advantage of the large XMCD effect associated with the Fe L edges with circular-polarization light[34]. In the XMCD-PEEM method the yield difference between opposite helicity of the beam is proportional to the dot product of the magnetization and the direction of the beam, which enables the mapping of an essentially in-plane component of surface magnetization. The samples were mounted with the long dot axis aligned perpendicular to the plane of incidence of the beam in order to highlight the magnetic contrast within the Neel cap.

As no external field can be applied during imaging the following protocol was used. The sample is subjected *ex situ* to a magnetic field of controlled magnitude using a calibrated electromagnet. It is then introduced under

vacuum, mounted on the microscope stage for imaging, and unmounted again to proceed again to an *ex situ* magnetization. Notice that the sample mounting differs at each stage leading to a different imaging location. Thus, the switching of Néel caps was not followed on given dots. Instead a statistical analysis over typically several tens of dots was performed at each stage to allow for a reliable estimation of the switching ratio to be determined.

### Acknowledgments

We gratefully acknowledge discussions with A. Marty, P. Bayle-Guillemaud, L. Buda-Prejbeanu, A. Masseboeuf, A. Thiaville.

### References


[1] Hirota, E., Sakakima, H. & Inomata, K. *Giant magnetoresistance devices*, vol. 40 of *Springer series in surface sciences* (Springer, Berlin, 2002).

[2] Zhu, J.-G., Zheng, Y. & Prinz, G. A. Ultrahigh density vertical magnetoresistive random access memory. *J. Appl. Phys.* **87**, 6668 (2000).

[3] Kikuchi, N., Okamoto, S., Kitakami, O. & Shimada, Y. Vertical bistable switching of spin vortex in a circular magnetic dot. *J. Appl. Phys.* **90**, 6548 (2001).

[4] Hubert, A. & Schäfer, R. *Magnetic domains. The analysis of magnetic microstructures* (Springer, Berlin, 1999).

[5] Arrott, A. S. Solving the selectivity problem in magnetic random access memories using configurations that form c-states. *Z. Metallkd.* **93**, 10 (2002).

[6] Okuno, T., Shigeto, K., Ono, T., Mibu, K. & Shinjo, T. Mfm study of magnetic vortex cores in circular permalloy dots: behavior in external field. *J. Magn. Magn. Mater.* **240**, 1–6 (2002).

[7] Shinjo, T., Okuno, T., Hassdorf, R., Shigeto, K. & Ono, T. Magnetic vortex core observation in circular dots of permalloy. *Science* **289**, 930 (2000).

[8] Van Waeyenberg, B. *et al.* Magnetic vortex core reversal by excitation with short bursts of an alternating field. *Nature* **444**, 461–464 (2006).

[9] Hertel, R., Gliga, S., Schneider, C. & Fähnle, M. Nanomagnetic toggle switching of vortex cores on the picosecond time scale. *Phys. Rev. Lett.* **98**, 117201 (2007).

[10] Xiao, Q. F., Rudge, J., Choi, B. C., Hong, Y. K. & Donohoe, G. Dynamics of vortex core switching in ferromagnetic nanodisks. *Appl. Phys. Lett.* **89**, 262507 (2006).

[11] Hubert, A. Stray-field-free magnetization configurations. *Phys. Stat. Sol.* **32**, 519–534 (1969).

[12] LaBonte, A. E. Two-dimensional bloch-type domain walls in ferromagnetic thin films. *J. Appl. Phys.* **40**, 2450–2458 (1969).

[13] Foss, S., Proksch, R., Dahlberg, E., Moskowitz, B. & Walsch, B. Localized micromagnetic perturbation of domain walls in magnetite using a magnetic force microscope. *Appl. Phys. Lett.* **69**, 3426–3428 (1996).

[14] Néel, L. Énergie des parois de bloch dans les couches minces. *C. R. Acad. Sci.* **241**, 533–536 (1955).

[15] Arrott, A. S. & Templeton, T. L. Micromagnetics and hysteresis as prototypes for complex systems. *Physica A* **233**, 259–271 (1997).

[16] Hertel, R. & Kronmüller, H. Computation of the magnetic domain structure in bulk permalloy. *Phys. Rev. B* **60**, 7366–7378 (1999).

[17] Jubert, P. O., Toussaint, J. C., Fruchart, O., Meyer, C. & Samson, Y. Flux-closure-domain states and demagnetizing energy determination in sub-micron size magnetic dots. *Europhys. Lett.* **63**, 132–138 (2003).

[18] Hertel, R. *et al.* Three-dimensional magnetic flux-closure patterns in mesoscopic fe islands. *Phys. Rev. B* **72**, 214409 (2005).

[19] Arrott, A. S., Heinrich, B. & Aharoni, A. Point singularities and magnetization reversal in ideally soft ferromagnetic cylinders. *IEEE Trans. Magn.* **15**, 1228 (1979).

[20] On the top views of FIG. 2b one can notice that antiparallel Néel caps found in asymmetric Bloch walls are nearly vertically-superimposed (*i.e.* shifted to the same side of the vertical core of the wall, see also FIG. 1e) whereas parallel Néel caps found in asymmetric Néel walls are shifted one with another, in fact they are on either side of the core of the domain wall. The lateral shift, which stems straighforwardly from a better closure of the magnetic flux, does play a minor role, if any, on the switching of a Néel cap.

[21] Fruchart, O. *et al.* Growth modes of fe(110) revisited: a contribution of self-assembly to magnetic materials. *J. Phys.: Condens. Matter* **19**, 053001 (2007).

[22] No contrast arising from the perpendicular magnetization orientation of the core of the Bloch wall can be ssen on our XMCD-PEEM images. The first reason is that the secondary electrons collected have a mean free path less than 10 nm, which is smaller than the thickness of Néel caps. The second reason is that our setup with a grazing incidence of the incoming photons is only weakly sensitive to perpendicular magnetization (see Methods). The polarity of the core of domain walls may however be deduced from the combined information of the direction of the magnetization in the top Néel cap and its shift towards $+y$ or $-y$, for the reasons explained in note[20]. The lateral shift can often be better appreciated at both extremities of the dot where it induces a strong asymmetry for positive versus negative $y$[18].

[23] Berger, L. Emission of spin waves by a magnetic multilayer traversed by a current. *Phys. Rev. B* **54**, 9353 (1996).

[24] Slonczewski, J. C. Current-driven excitation of magnetic multilayers. *J. Magn. Magn. Mater.* **159**, L1–L7 (1996).

[25] Cros, V. *et al.* Spin transfer torque: a new method to excite or reverse a magnetization. *C. R. Physique* **6**, 956–965 (2005).

[26] Arrott, A. S. Magnetic random access memories, browns paradox and hysterons. *J. Magn. Magn. Mater.* **258-259**, 25–28 (2003).

[27] Brownlie, C., McVitie, S., Chapman, J. N. & Wilkinson, C. D. W. Lorentz microscopy studies of domain wall trap structures. *J. Appl. Phys.* **100**, 033902 (2006).

[28] Shen, J., Zheng Gaib & Kirschner, J. Growth and magnetism of metallic thin films and multilayers by pulsed-laser deposition. *Surf. Sci. Rep.* **52**, 163–218 (2004).

[29] Fruchart, O., Jaren, S. & Rothman, J. Growth modes of w and mo thin epitaxial (110) films on (11$\bar{2}$0) sapphire. *Appl. Surf. Sci.* **135**, 218–232 (1998).

[30] Http://www.fftw.org.

[31] Ramstöck, K., Leibl, T. & Hubert, A. Optimizing stray field computations in finite-element micromagnetics. *J. Magn. Magn. Mater.* **135**, 97 (1994).

[32] Fruchart, O., Nozières, J.-P. & Givord, D. Growth and interface anisotropy of epitaxial mo/fe/mo(110) and w/fe/w(110) ultrathin films. *J. Magn. Magn. Mater.* **207**, 158–167 (1999).

[33] Bauer, E. Low energy electron microscopy. *Rep. Prog. Phys.* **57**, 895–938 (1994).

[34] Stöhr, J. Exploring the microscopic origin of magnetic anisotropies with x-ray magnetic circular dichroism (xmcd) spectroscopy. *J. Magn. Magn. Mater.* **200**, 470–497 (1999).